Polymorphism in a Multi-Component Crystal System of Trimesic Acid and *t*-Butylamine**

Yuncheng Yan,[1] Benson M. Kariuki,[1] Colan E. Hughes,[1] Andrew J. Logsdail,[2]

Kenneth D. M. Harris*[1]

1 School of Chemistry, Cardiff University, Park Place, Cardiff CF10 3AT, Wales, U.K.

2 Cardiff Catalysis Institute, School of Chemistry, Cardiff University, Park Place, Cardiff CF10 3AT, Wales, U.K.

* Author for correspondence: HarrisKDM@cardiff.ac.uk

** In memory of Professor Joel Bernstein, an inspirational pioneer in polymorphism research.

Abstract

Polymorphism in a multi-component crystal system of trimesic acid (TMA) and *t*-butylamine (TBA) with stoichiometry $(TMA)_2(TBA)_3$ is reported, with the discovery and structural characterization of two polymorphs with rhombohedral and triclinic symmetries. In each polymorph, the TBA molecules exist as protonated cations and the two independent TMA molecules are deprotonated by loss of a total of three protons (the specific protonation state of each TMA anion depends on the interpretation of hydrogen-bond disorder in the crystal structure). Both structures are based on sheets of TMA anions arranged in a hydrogen-bonded honeycomb network; these sheets are essentially planar in the rhombohedral polymorph but corrugated in the triclinic polymorph. The TBA cations are linked by hydrogen-bonding to the TMA anions in this network, with the *t*-butyl groups occupying the void space within the honeycomb network and the regions of space between adjacent sheets. Periodic DFT-D calculations suggest that the rhombohedral polymorph is more energetically stable than the triclinic polymorph.

Introduction

The diverse range of crystalline forms[1] that may exist for a given organic molecule includes polymorphs, co-crystals, solvates and hydrates. There is currently much interest in exploring the range of crystalline forms that are experimentally accessible for a given organic molecule, particularly with a view to rationalization of their structural features, understanding the relationships between their structural and physical properties, and establishing the transformation pathways that may exist for interconversion between different crystalline forms. Within this field of endeavour, the phenomenon of polymorphism[2-13] has received particular attention, recalling that polymorphs are defined as crystalline forms that have identical chemical composition but different structural properties.

In this paper, we use the general term *multi-component crystal* to describe a crystalline material that contains two or more different types of molecule, which may be neutral, cationic (e.g., as a result of protonation) or anionic (e.g., as a result of deprotonation). For polymorphism in multi-component organic molecular materials,[14,15] the different polymorphs contain the same types of molecule in an identical stoichiometric ratio, but have different crystal structures. Here we focus on polymorphism of multi-component crystals containing trimesic acid (benzene-1,3,5-tricarboxylic acid, TMA; Scheme 1) and *t*-butylamine (TBA; Scheme 1) in the stoichiometric ratio $(TMA)_2(TBA)_3$. We note that there is already an extensive literature on multi-component crystalline materials containing trimesic acid (either as the neutral TMA molecule or as anionic states formed by deprotonation of TMA), including hydrogen-bonded materials, metal-organic frameworks and solid inclusion compounds.[16-25]

The structural properties of multi-component crystals containing TMA and TBA are of interest from a number of viewpoints, including rationalization of how these materials achieve a balance between the formation of favourable hydrogen-bonding arrangements involving the strong hydrogen-bond donor and strong hydrogen-bond acceptor functionalities, while also accommodating the steric demands of the bulky *t*-butyl groups of the TMA molecules within the structure. Furthermore, recognizing that TMA molecules can exist in four different forms depending on the state of deprotonation[26,27] and that TBA molecules can exist in two different forms depending on the state of

protonation, there is potential for diversity (and unpredictability) in the nature of the hydrogen-bond donor and acceptor functionalities present in the crystal structure. In addition, the possibility that the hydrogen-bonding arrangements may be disordered creates the potential for a further level of structural complexity.

While we refer in general terms to *t*-butylamine as TBA and trimesic acid as TMA, it is important in certain contexts to define the specific state of deprotonation of the TMA molecules and the specific state of protonation of the TBA molecules. For this purpose, we denote the fully deprotonated TMA molecule (i.e., the benzene-1,3,5-tricarboxylate anion) as $\mathbf{tma}^{3-}$; the three types of anions corresponding to different degrees of deprotonation of TMA are then denoted $\mathrm{H_2}\mathbf{tma}^{-}$, $\mathrm{H}\mathbf{tma}^{2-}$ and $\mathbf{tma}^{3-}$, and the neutral TMA molecule is denoted $\mathrm{H_3}\mathbf{tma}$. Similarly, we denote the neutral *t*-butylamine molecule as **tba**, and the protonated TBA molecule is then denoted $\mathrm{H}\mathbf{tba}^{+}$. For a multi-component crystal containing TMA and TBA with stoichiometry $(\mathrm{TMA})_X(\mathrm{TBA})_Y$, the general formula specifying the detailed composition in terms of the state of deprotonation of the TMA molecules and the state of protonation of the TBA molecules is:

$$(\mathrm{H_3}\mathbf{tma})_{X-(x+y+z)}(\mathrm{H_2}\mathbf{tma}^{-})_x(\mathrm{H}\mathbf{tma}^{2-})_y(\mathbf{tma}^{3-})_z(\mathbf{tba})_{Y-(x+2y+3z)}(\mathrm{H}\mathbf{tba}^{+})_{x+2y+3z}$$

Clearly, if the material exhibits disorder in the hydrogen-bonding arrangement, this general formula may represent an over-simplification as the notation defined above assumes that each TMA molecule and each TBA molecule in the average crystal structure (as determined from diffraction-based techniques) contains an integer number of hydrogen atoms.

Herein, we report the discovery and structural properties of two polymorphs with stoichiometry $(\mathrm{TMA})_2(\mathrm{TBA})_3$, denoted polymorph I and polymorph II. Although the two polymorphs share some similarities in their structural features, they differ significantly in certain structural aspects. The energetic properties of the two polymorphs are also assessed on the basis of periodic DFT-D calculations.

Sample Preparation and Characterization

Polymorph I was obtained by three different procedures: (i) vapour diffusion of ethanol (or acetone) into a methanol solution containing TMA and TBA in 1:1 molar ratio at ambient

temperature, (ii) vapour diffusion of ethanol into a methanol solution containing TMA and TBA in 2:3 molar ratio at ambient temperature and (iii) vapour diffusion of ethanol or acetone into a methanol/water solution (molar ratio 10:1) containing TMA and TBA in 2:3 molar ratio at ambient temperature. Powder XRD confirmed that these preparation procedures produced monophasic samples of polymorph I.

Polymorph II was obtained following a crystallization process involving vapour diffusion of acetonitrile into a methanol solution containing TMA and TBA in 4:5 molar ratio at ambient temperature. This procedure led to the formation of a methanol solvate with composition $(TMA)_2(TBA)_2(MeOH)_1$ as the main phase. After collecting the crystals and leaving them in the open air for a few days, it was found that the majority of the sample had degraded into a polycrystalline phase (presumably due to loss of methanol and formation of a polycrystalline desolvated phase). However, some good-quality single crystals remained in the sample and were found by single-crystal XRD to be polymorph II of $(TMA)_2(TBA)_3$. A separate study[28] of desolvation of the methanol solvate phase $(TMA)_2(TBA)_2(MeOH)_1$ has shown that polymorph II of $(TMA)_2(TBA)_3$ is not formed as a product of the desolvation process; thus, the crystals of polymorph II of $(TMA)_2(TBA)_3$ found in the experimental procedure described above were most likely formed concomitantly as a minor crystallization product during the original crystallization of the methanol solvate phase.

Results and Discussion

The crystal structures of polymorph I and polymorph II of $(TMA)_2(TBA)_3$, determined from single-crystal XRD data, are shown in Figs. 1 – 4 and crystallographic data are given in Table 1. Following structure determination, simulation of the powder XRD pattern for polymorph I confirmed (see Fig. 5) that the structure determined from single-crystal XRD is representative of the experimental powder XRD patterns of the bulk polycrystalline samples obtained in the crystallization experiments described above. We note that a similar comparison between experimental and simulated powder XRD data could not be carried out for polymorph II, as only a very small amount of polymorph II was obtained as a minor phase within a mixed-phase sample, as described above.

Polymorph I is rhombohedral, with space group $R3c$. The asymmetric unit comprises two independent fragments of TMA (each corresponding to one third of a TMA molecule) and one

complete TBA molecule. Thus, the crystal structure contains two independent TMA molecules, each lying on a 3-fold symmetry axis (corresponding to a total of 2/3 TMA molecules in the asymmetric unit), and one independent TBA molecule.

Polymorph II is triclinic, with space group $P\bar{1}$. The asymmetric unit comprises two TMA molecules and three TBA molecules.

In each polymorph, all TBA molecules exist as protonated cations H**tba**$^+$ while, on average, the two independent TMA molecules are deprotonated by loss of a total of three protons. Thus, the two independent TMA anions have a total of three –CO_2H groups and three –CO_2^- groups. The exact state of deprotonation of each TMA anion depends on the interpretation of disorder in the hydrogen-bonding arrangements in the two crystal structures, as discussed in more detail below.

Polymorphs I and II adopt broadly similar structures, although with significant differences in certain features. Both polymorphs contain sheets of TMA anions arranged in a hydrogen-bonded honeycomb network parallel to the *ab*-plane (Figs. 1a and 2a). Within these honeycomb networks, each pair of adjacent molecules is linked by a ***single*** O–H···O hydrogen bond between a –CO_2H group in one molecule and a –CO_2^- group in the other molecule. Each "hexagon" of the honeycomb network is constructed from six –CO_2H···^-O_2C– hydrogen-bonded linkages of this type. The void space generated at the centre of the "hexagon" has an approximate diameter of *ca*. 10 Å in the plane of the honeycomb sheet.

The stacking of the honeycomb sheets along the *c*-axis is similar in polymorphs I and II, at least when viewed in projection along the *c*-axis. In each case, half the TMA anions within a given sheet are located directly above a TMA anion in the sheet below [for example, in both Fig. 1b and Fig. 2b, the TMA anion centred at (0, 0, *z*) in the sheet shown in red lies directly above a TMA anion centred at (0, 0, *z*′) in the sheet below shown in blue], whereas the other TMA anions in the sheet are located directly above a "hexagonal" void space in the honeycomb network in the sheet below [for example, in both Fig. 1b and Fig. 2b, the TMA anion centred at (2/3, 1/3, *z*) in the sheet shown in red lies directly above a void space centred at (2/3, 1/3, *z*′) in the sheet below shown in blue]. As the stacking of the honeycomb sheets is such that the void spaces in adjacent sheets are ***not*** located directly

above/below each other, the structures of polymorphs I and II do *not* contain continuous channels running parallel to the *c*-axis.

In polymorph I, the honeycomb sheets of TMA anions are essentially planar (Fig. 1c) and adjacent sheets are parallel to each other. In contrast, the honeycomb sheets of TMA anions in polymorph II are significantly corrugated (Fig. 2c) and the relationship between adjacent sheets is such that continuous channels (within the TMA substructure) running parallel to the *b*-axis are generated.

In each polymorph, the H**tba**$^+$ cations are linked by hydrogen-bonding to the TMA anions in the honeycomb network, with each –NH_3^+ group forming two N–H···O hydrogen bonds to oxygen atoms in a –$CO_2H\cdots{}^-O_2C$– hydrogen-bonded linkage formed between TMA anions (see Figs. 3a and 4a), giving a cyclic hydrogen-bonded array designated as either $R_3^2(8)$ or $R_3^3(8)$ in graph set notation[29] (Fig. 6). For each polymorph, these cyclic hydrogen-bonded arrays exhibit disorder between the $R_3^2(8)$ or $R_3^3(8)$ motifs, as discussed in more detail below. The directions from which the –NH_3^+ groups of the H**tba**$^+$ cations approach the honeycomb sheet in forming these cyclic hydrogen-bonded arrays (i.e. approaching from above, from below, or from the same plane as the sheet) and the orientations of the *t*-butyl groups of the H**tba**$^+$ cations relative to the sheet differ between the two polymorphs. In the case of polymorph II, these features also differ for the three independent H**tba**$^+$ cations in the asymmetric unit.

For polymorph I, which has one H**tba**$^+$ cation in the asymmetric unit, the CH_3–C–CH_3 unit of the H**tba**$^+$ cation lies very close to the plane of the honeycomb sheet of TMA anions. As a consequence of the crystal symmetry, a given "hexagonal" void space within the honeycomb sheet is occupied in this way by CH_3–C–CH_3 units from *three* H**tba**$^+$ cations. The other CH_3 group of the H**tba**$^+$ cation projects above the plane of the honeycomb sheet (see Fig. 3b), partially occupying the void space in the honeycomb sheet above. The –NH_3^+ group of the H**tba**$^+$ cation lies slightly below the plane of the honeycomb sheet (see Fig. 3b) and is oriented such that two N–H···O hydrogen bonds are formed (see Fig. 3a) with TMA anions in the honeycomb sheet, giving rise to cyclic hydrogen-bonded arrays discussed above. The other N–H bond of each H**tba**$^+$ cation is engaged in an N–H···O hydrogen bond to a TMA anion in the honeycomb sheet below (see Fig. 3b).

For polymorph II, the arrangement of H**tba**$^+$ cations relative to the honeycomb sheets of TMA anions is more complicated, as there are three independent H**tba**$^+$ cations in the asymmetric unit. Given the corrugated nature of the honeycomb sheets and the way in which they are stacked along the *c*-axis, a large void region is generated between a given pair of adjacent sheets (see Fig. 2c), which we describe as a channel (within the TMA substructure) running parallel to the *b*-axis. A pair of adjacent sheets (labelled as A and A' in Fig. 2c) that forms such channels are related to each other by the inversion symmetry operation. The location of the H**tba**$^+$ cations relative to the TMA anions is now discussed. As shown in Fig. 4a, the three independent H**tba**$^+$ cations interact with the –$CO_2H\cdots{}^-O_2C$– linkages in the honeycomb sheet of TMA anions, with each H**tba**$^+$ cation forming two N–H···O hydrogen bonds to a given –$CO_2H\cdots{}^-O_2C$– linkage, giving rise to cyclic hydrogen-bonded arrays discussed above. For two of the H**tba**$^+$ cations (labelled 1 and 2 in Fig. 4b), the –NH_3^+ group lies close to the "local plane" of the honeycomb sheet and the *t*-butyl group projects away from the sheet (downwards for sheets labelled A and upwards for sheets labelled A' in Fig. 4b); these *t*-butyl groups fill the space within the channels that exist between the two sheets in each A-A' pair. For these H**tba**$^+$ cations, one N–H bond of the –NH_3^+ group forms an N–H···O hydrogen bond with a TMA anion in an adjacent A-A' pair of sheets. For the other H**tba**$^+$ cation (labelled 3 in Fig. 4b), the CH_3–C–CH_3 unit lies close to the "local plane" of the honeycomb sheet, the other CH_3 group is projected away from the sheet (upwards for sheets labelled A and downwards for sheets labelled A' in Fig. 4b), and the –NH_3^+ group lies slightly out of the plane of the sheet. For this H**tba**$^+$ cation, one N–H bond of the –NH_3^+ group forms an N–H···O hydrogen bond with a TMA anion in the other sheet within the same A-A' pair.

Difference Fourier maps calculated during structure refinement suggested that, for each polymorph, the position of the hydrogen atom in each –$CO_2H\cdots{}^-O_2C$– hydrogen bond in the honeycomb sheets is disordered between –$CO_2H\cdots{}^-O_2C$– and –$CO_2^-\cdots HO_2C$– arrangements. For polymorph I, refinement of two hydrogen atom sites in each O–H···O linkage gives fractional occupancies of 0.73(7) and 0.27(7) for the two sites (in polymorph I, all O–H···O linkages are equivalent by symmetry). For polymorph II, there are three independent O–H···O linkages, and the refined fractional occupancies of the two hydrogen atom sites in each case are: 0.35(4)/0.65(4), 0.28(4)/0.72(4) and 0.35(4)/0.65(4), where the occupancies for the hydrogen atoms of one molecule

(denoted A) are given first and the occupancies for the hydrogen atoms of the other molecule (denoted B) are given second. Thus, the total number of $–CO_2H$ groups in molecule A is 0.98 and the total number of $–CO_2H$ groups in molecule B is 2.02, corresponding (within the estimated errors in determining the occupancies of the hydrogen atoms) to a description in which, *on average*, one TMA anion (molecule A) is of the type H**tma**$^{2–}$ and one TMA anion (molecule B) is of the type H_2**tma**$^{–}$.

Clearly, caution is required in considering the significance of hydrogen atom positions refined with fractional occupancies from X-ray diffraction data, given the low X-ray scattering power of hydrogen, and we therefore emphasize two factors in support of our assignment of disorder in the hydrogen-bonding arrangements in the present case. First, for all hydrogen atom positions in the disordered $–CO_2H\cdots{}^{-}O_2C–$ hydrogen bonds in polymorph I and polymorph II, the refined occupancies of the hydrogen atom positions differ from 0 or 1 (which would represent an ordered hydrogen-bonding arrangement) by more than 3 times the estimated standard deviations (esds) in the refined occupancies. Thus, for the disordered O–H···O hydrogen bond in polymorph I, the hydrogen site of lower occupancy has refined occupancy of 0.27(7) [3 × esd = 0.21], and for the three disordered O–H···O hydrogen bonds in polymorph II, the hydrogen sites of lower occupancy have refined occupancies of 0.35(4) [3 × esd = 0.12], 0.28(4) [3 × esd = 0.12] and 0.35(4) [3 × esd = 0.12].

Second, it is important to emphasize that disorder in O–H···O hydrogen bonds between carboxylic acid groups also has consequences for the single-bond *versus* double-bond character of the two C–O bonds of each carboxylic acid group, which is manifested in terms of the C–O bond distances in the average crystal structure determined from X-ray diffraction data. Clearly, in structure determination from X-ray diffraction data, the positions of the carbon and oxygen atoms are determined with greater reliably than the positions of the hydrogen atoms, and thus consideration of the C–O bond distances in the average crystal structure provides additional verification regarding disorder in the hydrogen-bonding arrangement. As shown in Table 2, for all the $–CO_2H\cdots{}^{-}O_2C–$ linkages in both polymorphs, the group with higher hydrogen atom occupancy has the longest C–OH bond and the shortest C=O bond, whereas the group with lower hydrogen atom occupancy has C–OH and C=O bond distances that tend to be closer to each other (and intermediate between the two values for the group with higher hydrogen atom occupancy). These observations are consistent with a

situation in which the group with higher hydrogen atom occupancy has greater $–CO_2H$ character and the group with lower hydrogen atom occupancy has greater $–CO_2^-$ character.

Focusing on the component of *higher* occupancy for each polymorph, there is a subtle difference between polymorphs I and II in the details of the hydrogen bonding within the cyclic hydrogen-bonded arrays that link the H**tba**$^+$ cations to the honeycomb sheets of TMA anions (see Figs. 3a and 4a). Thus, for polymorph I, the acceptors in the two N–H···O hydrogen bonds are an oxygen atom of the $–CO_2^-$ group and the C=O oxygen atom of the $–CO_2H$ group, corresponding to the $R_3^2(8)$ motif shown in Fig. 6a. In contrast, for polymorph II, the acceptors in the two N–H···O hydrogen bonds are an oxygen atom of the $–CO_2^-$ group and the OH oxygen atom of the $–CO_2H$ group, corresponding to the $R_3^3(8)$ motif shown in Fig. 6b. For the component of *lower* occupancy for each polymorph, the situation is reversed; thus, polymorph I exhibits the $R_3^3(8)$ motif and polymorph II exhibits the $R_3^2(8)$ motif.

The relative stabilities of the two polymorphs have been assessed using periodic DFT-D calculations. As discussed above, there is disorder in the position of the hydrogen atom in the O–H···O hydrogen bonds in each polymorph (representing both O–H···O and O···H–O hydrogen-bonding situations for the same oxygen atom positions) and it was therefore necessary to construct a suitable ordered model for each polymorph to allow the DFT-D calculations to be carried out. The ordered models were constructed by positioning a hydrogen atom (with full occupancy) in each O–H···O hydrogen bond at the site of *higher* occupancy in the disordered experimental structure. For each polymorph, the ordered model constructed in this manner has two distinct TMA molecules, with one molecule fully protonated (H_3**tma**) and the other molecule fully deprotonated (**tma**$^{3–}$). The overall stoichiometry is therefore (H_3**tma**)(**tma**$^{3–}$)(H**tba**$^+$)$_3$, which corresponds to $X = 2$, $Y = 3$, $x = 0$, $y = 0$, $z = 1$ in the general formula for multi-component TMA/TBA crystals given above.

Initially, periodic DFT-D geometry-optimization (with fixed unit cell) was carried out using the PBE-TS method for each polymorph, starting from the ordered structure derived from the experimentally determined structure, as discussed above. The energies of the resultant geometry-optimized structures were then calculated using the PBE-TS, PBE-MBD, PBE0-TS and PBE0-MBD methods. For all the calculation methods considered, the calculated energy is lower for polymorph I

than polymorph II, with the following energy differences [expressed per mole of the formula unit $(TMA)_2(TBA)_3$]: PBE-TS (10.7 kJ mol^{-1}), PBE-MBD (16.8 kJ mol^{-1}), PBE0-TS (9.7 kJ mol^{-1}), PBE0-MBD (14.8 kJ mol^{-1}). Among these methods, PBE0-MBD is considered[30,31] to give the most reliable assessment of the relative energies of polymorphs of organic materials. It is noteworthy that the MBD dispersion correction gives greater stability for polymorph I, relative to polymorph II, than the TS dispersion correction.

Periodic DFT-D geometry-optimization calculations (with fixed unit cell) were also carried out starting from an ordered structure for each polymorph constructed by positioning a hydrogen atom (with full occupancy) in each O–H···O hydrogen bond on the site of *lower* occupancy in the disordered experimental structure. For each polymorph, the geometry-optimization calculation led to transfer of the hydrogen atom to the other oxygen atom in the O–H···O hydrogen bond (i.e. O–H···O $\rightarrow$ O···H–O), thus effectively generating the high-occupancy ordered structure. Clearly, this observation supports the view that, for both polymorph I and polymorph II, the hydrogen atom position of higher occupancy in each O–H···O hydrogen bond in the experimental crystal structure corresponds to the energetically more stable hydrogen-bonding arrangement.

The results from our DFT-D calculations suggest that polymorph I is more stable than polymorph II, with the same conclusion reached from all four DFT-D methods used in this work. The relative stabilities among a set of polymorphs are often related to density, with higher density corresponding to greater stability, as conveyed by the so-called density rule.[32,33] In the present case, the densities calculated from the crystal structures at 296 K are 1.242 g cm^{-3} for polymorph I and 1.249 g cm^{-3} for polymorph II. Although the difference between the densities is small, it is nonetheless significant relative to the estimated errors in their determination (the estimated standard deviations in the calculated densities are *ca*. 0.0001 g cm^{-3} based on the estimated standard deviations in the unit cell volumes determined by single-crystal XRD). The polymorphism in the $(TMA)_2(TBA)_3$ system therefore represents a case in which the polymorph of lower density is the more stable polymorph (at least at 296 K).

Throughout our studies, no polymorphic phase transformations between polymorphs I and II were observed under ambient conditions. DSC measurements starting from polymorph I showed no

evidence for any thermal events on cooling/heating cycles (at 5 °C min^{-1}) from 20 °C → –100 °C → 20 °C and on heating/cooling cycles (at 10 °C min^{-1}) from 20 °C → 180 °C → 20 °C. In other DSC experiments on polymorph I, decomposition was observed on heating (at 10 °C min^{-1}) above *ca*. 200 °C. Unfortunately, DSC measurements starting from polymorph II could not be carried out due to the very small amount of polymorph II obtained in our work.

Concluding Remarks

The structural properties of the two polymorphs of $(TMA)_2(TBA)_3$ reported in this paper reveal an intriguing combination of similarities and differences, many of which may merit deeper investigation in due course. One particular aspect of interest concerns the disorder observed in the hydrogen-bonding arrangements in both polymorphs, as revealed in the crystal structures determined from single-crystal XRD data. However, recalling that the analysis of diffraction data delivers a space-averaged and time-averaged representation of the true structure, knowledge of the average crystal structure at a single temperature cannot distinguish whether the origin of the disorder in the hydrogen-bonding arrangements in these materials arises from static positional disorder or dynamic disorder. Other experimental strategies (particularly using spectroscopic techniques) and/or computational methods are required to provide more insights in this regard.

In addition to the possible occurrence of dynamic processes that may lead to interconversion between the hydrogen-bonding modes of major and minor occupancy discussed above, various other types of dynamic process may be envisaged for the $(TMA)_2(TBA)_3$ polymorphs, including 3-fold 120° jumps of the C–NH_3^+ groups (*via* rotation around the C–N bond) in the H**tba**$^+$ cations. It is important to note that this dynamic process is not revealed in terms of disordered hydrogen atom positions in the average crystal structure determined from diffraction-based techniques as the symmetry of the jump process matches the local symmetry of the C–NH_3^+ group. In contrast, solid-state NMR spectroscopy[34] can directly reveal the occurrence of this type of dynamic process, and has shown[34-36] that many hydrogen-bonded molecular crystals containing C–NH_3^+ groups (including zwitterionic amino acids) undergo the 3-fold 120° jump motion, in some cases with significant differences in the jump rate observed between different polymorphs.[35] Other dynamic processes that may be envisaged for the polymorphs of $(TMA)_2(TBA)_3$ include reorientational motions of the *t*-

butyl groups and methyl groups, which are also readily investigated using solid-state NMR techniques.[37-39]

In the context of assessing the relative energetic properties of polymorphs using periodic DFT-D calculations on crystal structures determined from diffraction-based techniques, we emphasize that such calculations do not take into consideration the various types of dynamic process that may occur in the material. Clearly, the different entropic contributions arising from differences in the dynamic properties between different polymorphs may have a significant influence on their relative energetic stabilities.

Methods

Single-crystal XRD data for polymorph I were recorded on a Nonius Kappa CCD diffractometer using Mo Kα radiation (λ = 0.71073 Å). Single-crystal XRD data for polymorph II were recorded on an Agilent SuperNova Dual Atlas diffractometer with a mirror monochromator using Cu Kα radiation (λ = 1.5418 Å) radiation. Crystal structures were solved using SHELXS[40] and refined using SHELXL.[41] For non-hydrogen atoms, anisotropic displacement parameters were refined. The hydrogen atoms bonded to the aromatic rings of TMA were inserted in idealized positions and a riding model was used with U_{iso} for each hydrogen atom set to 1.2 times the value of U_{eq} for the atom to which it is bonded. Idealized geometry was also used for each hydrogen atom of TBA, with U_{iso} set to 1.5 times the value of U_{eq} for the atom to which it is bonded, with free rotation about the C–CH_3 and C–NH_3^+ bonds. A disordered model was used for hydrogen atoms involved in –CO_2H···$^-O_2$C– hydrogen bonds, with the hydrogen atom allowed to occupy two positions with fractional occupancies, corresponding to disorder between –CO_2H···$^-O_2$C– and –CO_2^-···HO_2C– hydrogen-bonding arrangements. For a given hydrogen-bonded linkage, the total occupancy of the two hydrogen atom positions was constrained to be equal to 1. For polymorph I, one hydrogen atom is disordered between two sites, with the following occupancies: H2/H4A, 0.73(7)/0.27(7). For polymorph II, there are three independent –CO_2H···$^-O_2$C– hydrogen-bonded linkages; in each case, the hydrogen atom is disordered between two sites, with the following occupancies: H1/H11A, 0.72(4)/0.28(4); H3/H7, 0.65(4)/0.35(4); H5/H9, 0.65(4)/0.35(4).

Powder XRD data were recorded at ambient temperature on a Bruker D8 instrument operating in transmission mode using CuKα_1 radiation (Ge monochromated).

Differential scanning calorimetry (DSC) data were recorded using a TA Instruments Q100 differential scanning calorimeter, with the powder sample loaded in a hermetically sealed aluminium pan. DSC data were recorded at heating/cooling rates of 5 °C min^{-1} or 10 °C min^{-1}.

Density functional theory (DFT) calculations on the experimentally determined crystal structures were carried out using FHI-aims[42-44] (date stamp: 190813). Geometry optimization calculations used the PBE version of the general gradient approximation (GGA) coupled with the Tkatchenko-Scheffler (TS) dispersion correction.[45,46] Due to the disorder of the hydrogen sites in the O–H···O hydrogen bonds in both polymorphs, it was necessary for the DFT calculations to consider ordered hydrogen-bonding arrangements, as discussed in the text.

Following geometry optimization, energy calculations were carried out using both GGA and hybrid-GGA exchange-correlation functionals, specifically PBE[45] and PBE0,[47] coupled with either the TS method[46] or the many-body dispersion (MBD)[48] method for dispersion correction. Thus, the complete set of exchange-correlation functionals considered in this work were: PBE-TS, PBE-MBD, PBE0-TS and PBE0-MBD. The electronic structure calculations were carried out with an "intermediate" basis set and relativistic effects were included *via* the scaled zeroth order regular approximation.[42] A Γ-centred *k*-grid was used with a minimum sample spacing of 0.05 Å^{-1}; testing with a denser *k*-grid sampling of 0.04 Å^{-1} gave changes in relative energies of < 2 meV. The electronic structure self-consistent field (SCF) cycle was converged when changes in the electron density, the total energy and the sum of the eigenvalue energies were below 10^{-6} e a_0^{-3}, 10^{-6} eV and 10^{-6} eV, respectively.

Associated Content

Supporting Information

Crystallographic information (cif files) for polymorph I and polymorph II of $(TMA)_2(TBA)_3$.

Accession Codes

CCDC 1977369−1977370 contain the supplementary crystallographic data for this paper. These data can be obtained free of charge via www.ccdc.cam.ac.uk/data_request/cif, or by emailing data_request@ccdc.cam.ac.uk, or by contacting The Cambridge Crystallographic Data Centre, 12 Union Road, Cambridge CB2 1EZ, UK; fax: +44 1223 336033.

Author Information

Corresponding Author

*E-mail: HarrisKDM@cardiff.ac.uk

ORCID

Kenneth D. M. Harris: 0000-0001-7855-8598

Benson M. Kariuki: 0000-0002-8658-3897

Notes

The authors declare no competing financial interest.

Acknowledgements

We are grateful to Cardiff University for financial support (studentship to Y. Y.). We thank the U. K. High Performance Computing "Materials Chemistry Consortium" (EP/R029431), for providing access to the ARCHER National Supercomputing Service, and Supercomputing Wales for access to the Hawk HPC facility, which is part-funded by the European Regional Development Fund *via* the Welsh Government.

Table 1: Crystallographic data and refinement parameters for polymorph I and polymorph II of $(TMA)_2(TBA)_3$.

	Polymorph I	Polymorph II
Crystal System	rhombohedral	triclinic
Space Group	R3c	$P\bar{1}$
T / K	296(2)	296(2)
F_w	639.69	639.69
a / Å	16.7282(7)	16.2289(6)
b / Å	16.7282(7)	16.4533(6)
c / Å	21.1828(6)	7.3526(3)
α / °	90	92.246(3)
β / °	90	95.790(3)
γ / °	120	118.901(4)
V / Å^3	5133.5(5)	1701.26(13)
Z	6	2
Crystal size / mm^3	0.40 × 0.40 × 0.15	0.22 × 0.10 × 0.09
No. of reflections	8660	12272
No. of independent reflections	2530	6646
No. of parameters	142	424
R(int)	0.0461	0.0211
R1	0.0420	0.0542
wR2	0.0889	0.1483

Table 2: Lengths of the C–O bonds and hydrogen atom occupancies in the carboxylic acid/carboxylate groups in polymorphs I and II (the atom numbering corresponds to that in the deposited cif files).

Polymorph I		
	C–O Distance	H occupancy
C(3)–O(1)	1.227(3) Å	
C(3)–O(2)–H(2)	1.285(3) Å	0.73(7)
C(6)–O(3)	1.237(3) Å	
C(6)–O(4)–H(4A)	1.280(3) Å	0.27(7)
Polymorph II		
	C–O Distance	H occupancy
C(7)–O(2)	1.205(2) Å	
C(7)–O(1)–H(1)	1.317(2) Å	0.72(4)
C(18)–O(12)	1.235(2) Å	
C(18)–O(11)–H(11A)	1.265(2) Å	0.28(4)
C(8)–O(4)	1.205(2) Å	
C(8)–O(3)–H(3)	1.307(2) Å	0.65(4)
C(16)–O(8)	1.232(2) Å	
C(16)–O(7)–H(7)	1.268(2) Å	0.35(4)
C(9)–O(6)	1.206(2) Å	
C(9)–O(5)–H(5)	1.312(2) Å	0.65(4)
C(17)-O(10)	1.233(2) Å	
C(17)–O(9)–H(9)	1.268(2) Å	0.35(4)

References

1. Grothe, E.; Meekes, H.; Vlieg, E.; ter Horst, J. H.; de Gelder, R. Solvates, salts, and cocrystals: a proposal for a feasible classification system. *Cryst. Growth Des.* **2016**, *16*, 3237-3243.

2. Bernstein, J. *Polymorphism in Molecular Crystals*. Oxford University Press: Oxford, 2002.

3. Blagden, N.; Davey, R. J. Polymorph selection: challenges for the future? *Cryst. Growth Des.* **2003**, *3*, 873-885.

4. Rodriguez-Spong, B.; Price, C. P.; Jayasankar, A.; Matzger, A. J.; Rodriguez-Hornedo, N. General principles of pharmaceutical solid polymorphism: a supramolecular perspective. *Adv. Drug. Deliver. Rev.* **2004**, *56*, 241-274.

5. Braga, D.; Grepioni, F. Making crystals from crystals: a green route to crystal engineering and polymorphism. *Chem. Commun.* **2005**, 3635-3645.

6. Bernstein, J. Cultivating crystal forms. *Chem. Commun.* **2005**, 5007-5012.

7. Chen, S. A.; Xi, H. M.; Yu, L. Cross-nucleation between ROY polymorphs. *J. Am. Chem. Soc.* **2005**, *127*, 17439-17444.

8. Ahn, S.; Guo, F.; Kariuki, B. M.; Harris, K. D. M. Abundant polymorphism in a system with multiple hydrogen-bonding opportunities: oxalyl dihydrazide. *J. Am. Chem. Soc.* **2006**, *128*, 8441-8452.

9. Price, S. L. Computed crystal energy landscapes for understanding and predicting organic crystal structures and polymorphism. *Acc. Chem. Res.* **2009**, *42*, 117-126.

10. Bernstein, J. Polymorphism − a perspective. *Cryst. Growth Des.* **2011**, *11*, 632-650.

11. Williams, P. A.; Hughes, C. E.; Lim, G. K.; Kariuki, B. M.; Harris, K. D. M. Discovery of a new system exhibiting abundant polymorphism: *m*-aminobenzoic acid. *Cryst. Growth Des.* **2012**, *12*, 3104-3113.

12. Cruz-Cabeza, A. J.; Reutzel-Edens, S. M.; Bernstein, J. Facts and fictions about polymorphism. *Chem. Soc. Rev.* **2015**, *44*, 8619-8635.

13. Al Rahal, O.; Hughes, C. E.; Williams, P. A.; Logsdail, A. J.; Diskin-Posner, Y.; Harris, K. D. M. Polymorphism of L-tryptophan. *Angew. Chem. Int. Ed.* **2019**, *58*, 18788-18792.

14. Aitipamula, S.; Chow, P. S.; Tan, R. B. H. Polymorphism in cocrystals: a review and assessment of its significance. *CrystEngComm* **2014**, *16*, 3451-3465.

15. Prohens, R.; Barbas, R.; Portell, A.; Font-Bardia, M.; Alcobe, X.; Puigjaner, C. Polymorphism of cocrystals: the promiscuous behavior of agomelatine. *Cryst. Growth Des.* **2016**, *16*, 1063-1070.

16. Herbstein, F. H.; Kapon, M.; Reisner, G. M. Catenated and non-catenated inclusion complexes of trimesic acid. *J. Inclusion Phenom.* **1987**, *5*, 211-214.

17. Herbstein, F. H. Structural parsimony and structural variety among inclusion complexes (with particular reference to the inclusion compounds of trimesic acid, N-(*p*-tolyl)-tetrachlorophthalimide, and the heilbron "complexes"). *Top. Curr. Chem.* **1987**, *140*, 107-139.

18. Melendez, R. E.; Sharma, C. V. K.; Zaworotko, M. J.; Bauer, C.; Rogers, R. D. Toward the design of porous organic solids: modular honeycomb grids sustained by anions of trimesic acid. *Angew. Chem. Int. Ed.* **1996**, *35*, 2213-2215.

19. Sharma, C. V. K.; Bauer, C. B.; Rogers, R. D.; Zaworotko, M. J. Interdigitated supramolecular laminates. *Chem. Commun.* **1997**, 1559-1560.

20. Biradha, K.; Dennis, D.; MacKinnon, V. A.; Sharma, C. V. K.; Zaworotko, M. J. Supramolecular synthesis of organic laminates with affinity for aromatic guests: a new class of clay mimics. *J. Am. Chem. Soc.* **1998**, *120*, 11894-11903.

21. Zaworotko M. J. Superstructural diversity in two dimensions: crystal engineering of laminated solids. *Chem. Commun.* **2001**, 1-9.

22. Shattock, T. R.; Vishweshwar, P.; Wang, Z. Q.; Zaworotko M. J. 18-Fold interpenetration and concomitant polymorphism in the 2:3 co-crystal of trimesic acid and 1,2-bis(4-pyridyl)ethane. *Cryst. Growth Des.* **2005**, *5*, 2046-2049.

23. Fujii, K.; Ashida, Y.; Uekusa, H.; Hirano, S.; Toyota, S.; Toda, F.; Pan, Z.; Harris, K. D. M. Vapour induced crystalline transformation investigated by *ab initio* powder X-ray diffraction analysis. *Cryst. Growth Des.* **2009**, *9*, 1201-1207.

24. Ivasenko, O.; Perepichka, D. F. Mastering fundamentals of supramolecular design with carboxylic acids. Common lessons from X-ray crystallography and scanning tunneling microscopy. *Chem. Soc. Rev.* **2011**, *40*, 191-206.

25. Yan, Y.; Hughes, C. E.; Kariuki, B. M.; Harris, K. D. M. A rare case of polymorphism in a three-component co-crystal system, with each polymorph having ten independent molecules in the asymmetric unit. *Cryst. Growth Des.* **2013**, *13*, 27-30.

26. Duchamp, D. J.; Marsh, R. E. The crystal structure of trimesic acid (benzene-1,3,5-tricarboxylic acid). *Acta Crystallogr. Sect. B* **1969**, *25*, 5-19.

27. Herbstein, F. H.; Kapon, M.; Reisner, G. M. Trimesic acid, its hydrates, complexes and polymorphism. VIII. Interstitial complexes of α- and (the hypothetical) γ-trimesic acid. *Acta Crystallogr. Sect. B* **1985**, *41*, 348-354.

28. In separate research focused on the methanol solvate phase $(TMA)_2(TBA)_2(MeOH)_1$, it has been shown [Y. Yan, C. E. Hughes, B. M. Kariuki, K. D. M. Harris, *paper in preparation*] that desolvation of the methanol solvate produces a non-solvate material with the same 1:1 TMA:TBA stoichiometry as the methanol solvate, and with no evidence for the formation of polymorph II of $(TMA)_2(TBA)_3$ as a product of the desolvation process. Thus, it is most likely that the crystals of polymorph II of $(TMA)_2(TBA)_3$ found in the experimental procedure described here were produced concomitantly, as a minor crystallization product, in the original crystallization of the methanol solvate.

29. Etter, M. C.; MacDonald, J. C.; Bernstein, J. Graph-set analysis of hydrogen-bond patterns in organic crystals. *Acta Crystallogr. Sect. B* **1990**, *46*, 256-262.

30. Shtukenberg, A. G.; Zhu, Q.; Carter, D. J.; Vogt, L.; Hoja, J.; Schneider, E.; Song, H.; Pokroy, B.; Polishchuk, I.; Tkatchenko, A.; Oganov, A. R.; Rohl, A. L.; Tuckerman, M. E.; Kahr, B. Powder diffraction and crystal structure prediction identify four new coumarin polymorphs. *Chem. Sci.* **2017**, *8*, 4926-4940.

31. Hoja, J.; Ko, H. Y.; Neumann, M. A.; Car, R.; DiStasio, R. A.; Tkatchenko, A. Reliable and practical computational description of molecular crystal polymorphs. *Science Advances* **2019**, *5*, eaau3338.

32. Burger, A.; Ramberger, R. On the polymorphism of pharmaceuticals and other molecular crystals. I. *Mikrochim. Acta* **1979**, *2*, 259-271.

33. Burger, A.; Ramberger, R. On the polymorphism of pharmaceuticals and other molecular crystals. II. *Mikrochim. Acta* **1979**, *2*, 273-316.

34. Aliev, A. E.; Harris, K. D. M. Probing hydrogen bonding in solids using solid state NMR spectroscopy. *Struct. Bond.* **2004**, *108*, 1-53.

35. Kitchin, S. J.; Ahn, S.; Harris, K. D. M. Effects of polymorphism on functional group dynamics: solid state ^{2}H NMR studies of the dynamic properties of the α and β phases of L-glutamic acid. *J. Phys. Chem. A* **2002**, *106*, 7228-7234.

36. Kitchin, S. J.; Tutoveanu, G.; Steele, M. R.; Porter, E. L.; Harris, K. D. M. Significantly contrasting solid state dynamics of the racemic and enantiomerically pure crystalline forms of an amino acid. *J. Phys. Chem. B* **2005**, *109*, 22808-22813.

37. Clough, S.; Heidemann, A.; Horsewill, A. J.; Lewis, J. D.; Paley, M. N. J. The rate of thermally activated methyl group rotation in solids. *J. Phys. C Solid State Phys.* **1982**, *15*, 2495-2508.

38. Riddell, F. G.; Arumugam, S.; Harris, K. D. M.; Rogerson, M.; Strange, J. H. A ^{13}C CP/MAS NMR study of a double *tert*-butyl group rotation in the solid state using $T_{1\rho}$ and line shape measurements. *J. Am. Chem. Soc.* **1993**, *115*, 1881-1885.

39. Beckmann, P. A.; Alhallaq, H. A.; Fry, A. M.; Plofker, A. L.; Roe, B. A.; Weiss, J. A. Solid state proton spin relaxation and methyl and *t*-butyl reorientation. *J. Chem. Phys.* **1994**, *100*, 752-753.

40. Sheldrick, G. M. A short history of *SHELX*. *Acta Crystallogr. Sect. A* **2008**, *64*, 112-122.

41. Sheldrick, G. M. Crystal structure refinement with *SHELXL*. *Acta Crystallogr. Sect. C* **2015**, *71*, 3-8.

42. Blum, V.; Gehrke, R.; Hanke, F.; Havu, P.; Havu, V.; Ren, X.; Reuter, K.; Scheffler, M. *Ab initio* molecular simulations with numeric atom-centered orbitals. *Comp. Phys. Commun.* **2009**, *180*, 2175-2196.

43. Ren, X.; Rinke, P.; Blum, V.; Wieferink, J.; Tkatchenko, A.; Sanfilippo, A.; Reuter, K.; Scheffler, M. Resolution-of-identity approach to Hartree-Fock, hybrid density functionals, RPA, MP2 and *GW* with numeric atom-centered orbital basis functions. *New J. Phys.* **2012**, *14*, 053020.

44. Levchenko, S. V.; Ren, X.; Wieferink, J.; Johanni, R.; Rinke, P.; Blum, V.; Scheffler, M. Hybrid functionals for large periodic systems in an all-electron, numeric atom-centered basis framework. *Comp. Phys. Commun.* **2015**, *192*, 60-69.

45. Perdew, J. P.; Burke, K.; Ernzerhof, M. Generalized gradient approximation made simple. *Phys. Rev. Lett.* **1996**, *77*, 3865-3868.

46. Tkatchenko, A.; Scheffler, M. Accurate molecular van der Waals interactions from ground-state electron density and free-atom reference data. *Phys. Rev. Lett.* **2009**, *102*, 073005.

47. Adamo, C.; Barone, V. Toward reliable density functional methods without adjustable parameters: the PBE0 model. *J. Chem. Phys.* **1999**, *110*, 6158-6170.

48. Ambrosetti, A.; Reilly, A. M.; DiStasio, R. A.; Tkatchenko, A. Long-range correlation energy calculated from coupled atomic response functions. *J. Chem. Phys.* **2014**, *140*, 18A508.

Figures

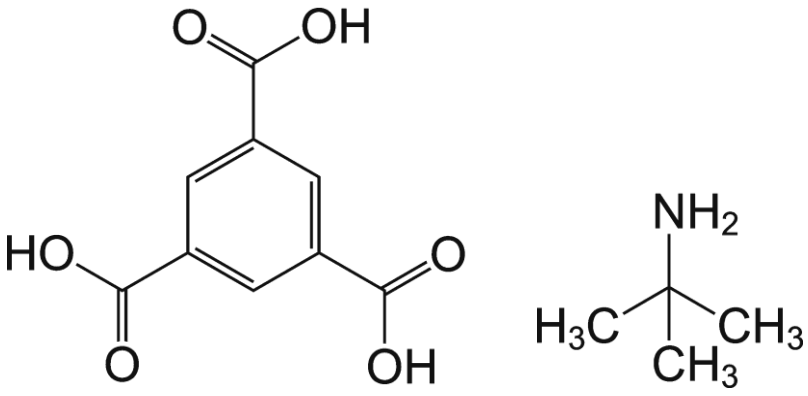

Scheme 1. Molecular structures of TMA (left) and TBA (right).

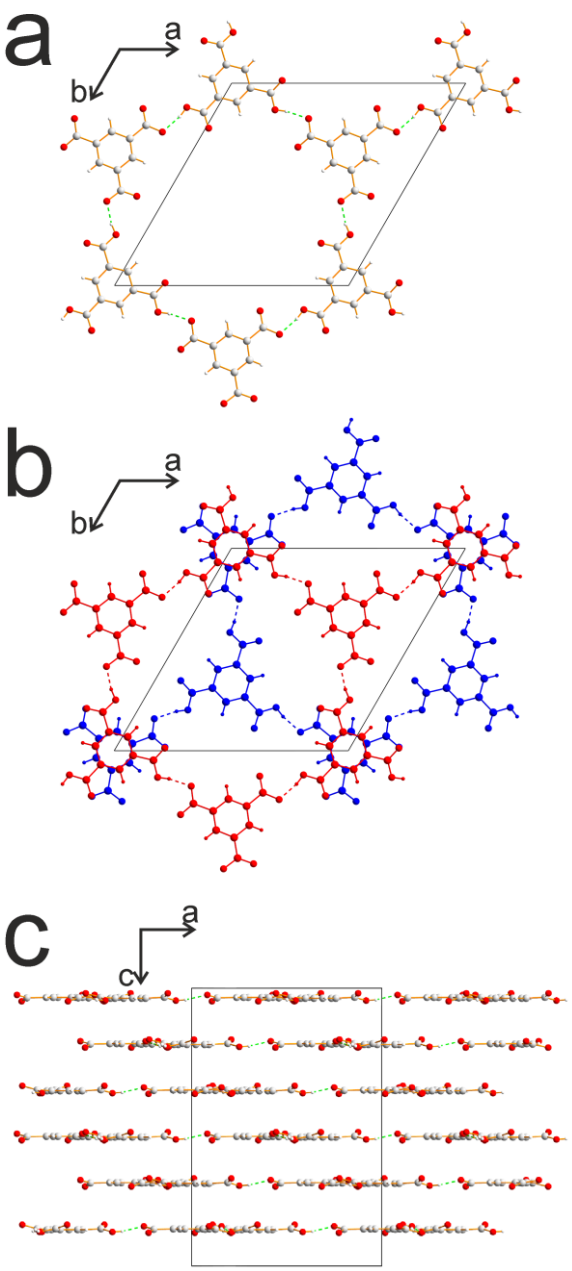

Figure 1. Arrangement of TMA anions in the crystal structure of polymorph I of $(TMA)_2(TBA)_3$ showing: (a) a single hydrogen-bonded sheet of TMA anions arranged in a honeycomb network parallel to the *ab*-plane, (b) the relationship between two adjacent hydrogen-bonded sheets (shown in blue and red), and (c) the stacking of sheets of TMA anions along the *c*-axis viewed (along the *b*-axis) parallel to the plane of the sheets. For each O–H···O hydrogen bond, only the hydrogen atom position of higher occupancy is shown. Hydrogen bonds are indicated by dashed lines.

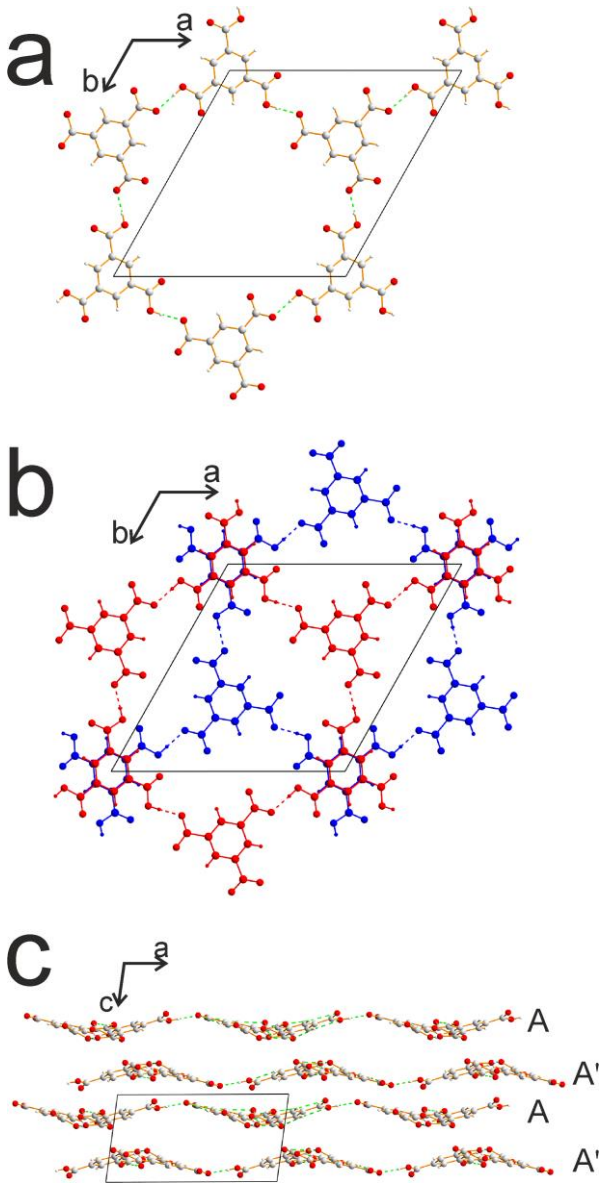

Figure 2. Arrangement of TMA anions in the crystal structure of polymorph II of $(TMA)_2(TBA)_3$ showing: (a) a single hydrogen-bonded sheet of TMA anions arranged in a honeycomb network, (b) the relationship between two adjacent hydrogen-bonded sheets (shown in blue and red), and (c) the stacking of sheets of TMA anions along the *c*-axis viewed (along the *b*-axis) parallel to the average plane of the sheets. For each O–H···O hydrogen bond, only the hydrogen atom position of higher occupancy is shown. In (c), the labelling of the layers of TMA anions (as A and A') is discussed in the text. Hydrogen bonds are indicated by dashed lines.

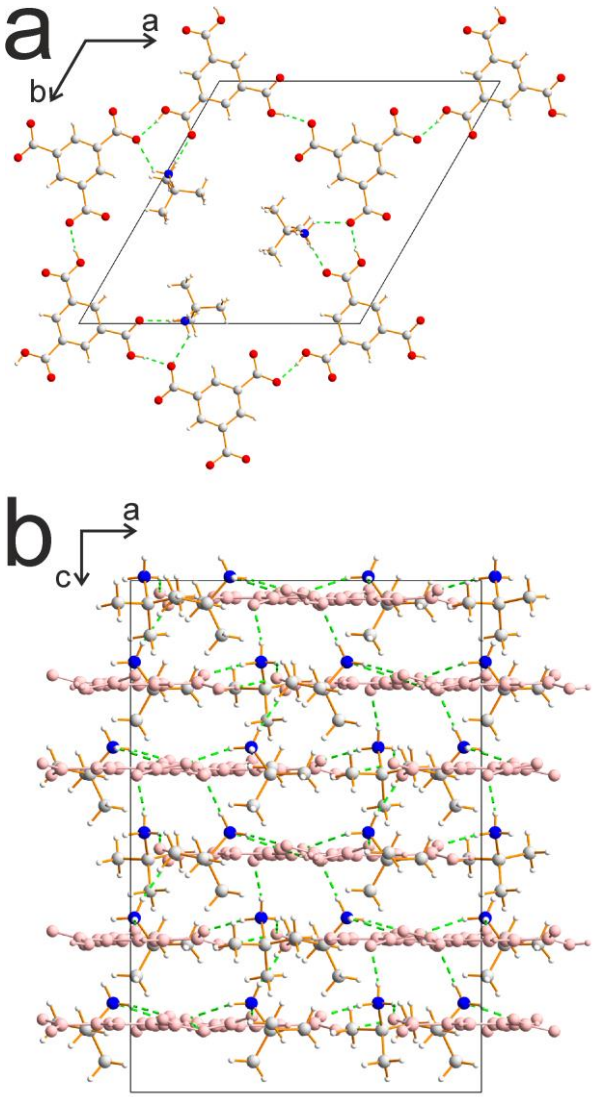

Figure 3. Crystal structure of polymorph I of $(TMA)_2(TBA)_3$ showing: (a) the set of three TBA cations located within the "hexagonal" void space in the honeycomb network of TMA anions, and (b) the complete crystal structure viewed (along the *b*-axis) parallel to the plane of the sheets of TMA anions. To make it easier to identify the locations of the TBA cations, all TMA anions are displayed in pink. In (a), only the hydrogen atom position of higher occupancy in each O–H···O hydrogen bond is shown. Hydrogen bonds are indicated by green dashed lines.

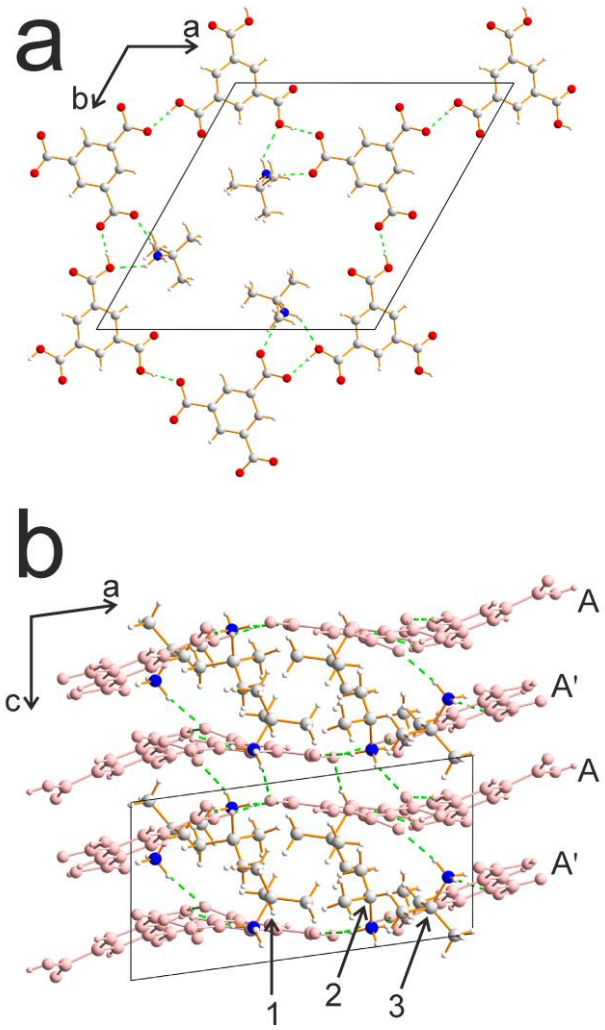

Figure 4. Crystal structure of polymorph II of $(TMA)_2(TBA)_3$ showing: (a) the set of three TBA cations located within the "hexagonal" void space in the honeycomb network of TMA anions, and (b) the complete crystal structure viewed (along the *b*-axis) parallel to the plane of the sheets of TMA anions. To make it easier to identify the locations of the TBA cations, all TMA anions are displayed in pink. In (a), only the hydrogen atom position of higher occupancy in each O–H···O hydrogen bond is shown. In (b), the labelling of the layers of TMA anions (as A and A') and the labelling of the three independent TBA cations (as 1, 2 and 3) are discussed in the text. Hydrogen bonds are indicated by green dashed lines.

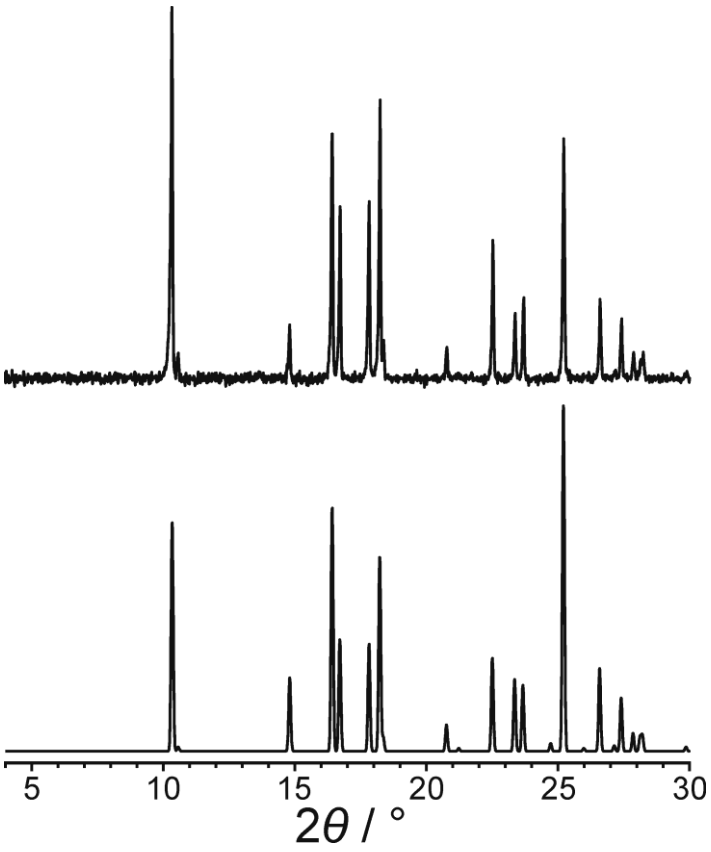

Figure 5. Top: experimental powder XRD data for a bulk polycrystalline sample of polymorph I of $(TMA)_2(TBA)_3$. Bottom: powder XRD pattern simulated from the crystal structure of polymorph I of $(TMA)_2(TBA)_3$ determined from single-crystal XRD.

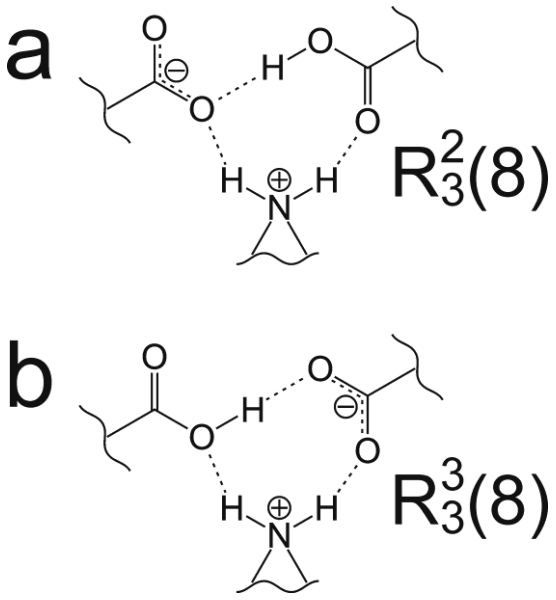

Figure 6. The two different cyclic hydrogen-bonding arrangements linking the TBA cations to the honeycomb sheets of TMA anions, designated in graph set notation as (a) $R_3^2(8)$ and (b) $R_3^3(8)$.

For Table of Contents Use Only

Polymorphism in a Multi-Component Crystal System of Trimesic Acid and *t*-Butylamine

Yuncheng Yan, Benson M. Kariuki, Colan E. Hughes, Andrew J. Logsdail, Kenneth D. M. Harris*

TOC Graphic

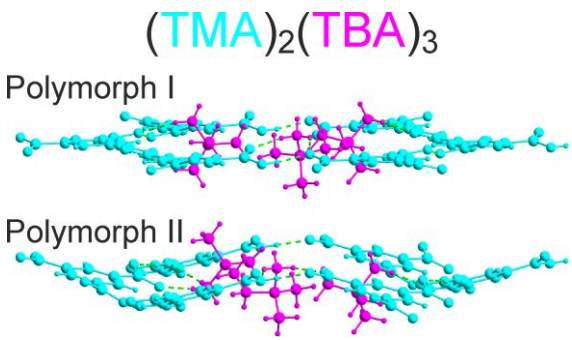

Synopsis

Two polymorphs of multi-component crystals containing trimesic acid (TMA) and *t*-butylamine (TBA) in the stoichiometric ratio $(TMA)_2(TBA)_3$ are reported, with structural properties determined from single-crystal X-ray diffraction. The similarities and differences between the structural features of the two polymorphs are elucidated, and their relative energetic properties are assessed on the basis of periodic DFT-D calculations.